

## Unveiling Temporal Correlations Characteristic of a Phase Transition in the Output Intensity of a Fiber Laser

A. Aragonese,<sup>1,2</sup> L. Carpi,<sup>1</sup> N. Tarasov,<sup>3,4</sup> D. V. Churkin,<sup>3,5,6</sup> M. C. Torrent,<sup>1</sup> C. Masoller,<sup>1</sup> and S. K. Turitsyn<sup>3,6</sup>

<sup>1</sup>*Departament de Física, Universitat Politècnica de Catalunya, 08222 Terrassa, Spain*

<sup>2</sup>*Duke University, Physics Department, Box 90305, Durham, North Carolina 27708, USA*

<sup>3</sup>*Aston Institute of Photonic Technologies, Aston University, Birmingham B4 7ET, United Kingdom*

<sup>4</sup>*Institute for Computational Technologies, SB RAS, Novosibirsk 630090, Russia*

<sup>5</sup>*Institute of Automation and Electrometry SB RAS, Novosibirsk 630090, Russia*

<sup>6</sup>*Novosibirsk State University, Novosibirsk 630090, Russia*

(Received 20 May 2015; published 22 January 2016)

We use advanced statistical tools of time-series analysis to characterize the dynamical complexity of the transition to optical wave turbulence in a fiber laser. Ordinal analysis and the horizontal visibility graph applied to the experimentally measured laser output intensity reveal the presence of temporal correlations during the transition from the laminar to the turbulent lasing regimes. Both methods unveil coherent structures with well-defined time scales and strong correlations both, in the timing of the laser pulses and in their peak intensities. Our approach is generic and may be used in other complex systems that undergo similar transitions involving the generation of extreme fluctuations.

DOI: 10.1103/PhysRevLett.116.033902

Fiber lasers are important practical devices that represent complex nonlinear systems with many degrees of freedom [1–4]. Typically, the output of a fiber laser involves nonlinear interactions of millions of longitudinal cavity modes in regimes far from thermal equilibrium [5]. In general, wave dynamics in fiber lasers is highly complex, as in other optical wave turbulence systems [6,7]. Though the underlying physical effect, nonlinear four-wave mixing, is purely deterministic and well understood, it is also well known that due to a huge number of nonlinearly interacting elementary modes (up to hundreds of millions) a direct dynamical description is not fully adequate in this problem (see, e.g., Refs. [6–8] and references therein), and statistical tools, such as entropy and complexity measures should be used to characterize the complex fluctuations in the generated output signals. Within this framework of wave turbulence, the role of “temperature” is played by optical noise that occurs in the gain medium, which in fiber lasers leads to an effective “nonlinear noise” due to four-wave-mixing.

Recently, the analogy between hydrodynamic transition to turbulence and change of operational regimes in fiber lasers has been studied experimentally and theoretically [8]. Such transition, being a relevant example of a phase transition in a 1D physical system, was shown to be accompanied by the occurrence of coherent spatiotemporal structures.

In this work we address an important question relevant to practical identification of such structures: are there underlying correlations and/or specific time scales in the easily measurable intensity fluctuations of laser radiation? In order to investigate this issue we use two nonlinear analysis

tools: ordinal analysis [9] and the horizontal visibility graph [10]. Our motivation is that these methods have been widely used to analyze the observed output signals of complex systems. They have been able to provide new information, such as the identification of frequent and/or missing patterns in the data, the classification of different behaviors, the characterization of deterministic and stochastic events, etc. [11–19]. Here we show that they both provide consistent information, allowing us to clearly identify the presence of long-range temporal correlations in the experimentally measured laser output intensity.

In our experiments, we measure an output temporal intensity dynamics of a quasi-cw Raman fiber laser formed of 1 km of normal dispersion fiber placed between two fiber Bragg gratings acting as cavity mirrors [8]. State-of-the-art experimental capabilities allowed us to register extremely long time traces with total number of intensity data points of  $50 \times 10^6$ . Taking into account the discretization time of 12.5 ps, the intensity dynamics over 625  $\mu$ s could be captured. In order to be able to compare among time series recorded at different pump power, each time series is normalized to have zero mean and unit variance. Depending on power, the generation regime can be considered as “laminar” or “turbulent” [8]. The transition occurs at pump power 0.9 W (see Ref. [8] for details). Despite the radically different coherence properties of radiation in these two regimes, the output intensity  $I(t)$  looks similar and irregular at all powers, as seen in Fig. 1(a), with typical intensity probability distribution function (PDF) of intensity values,  $p[I(t)]$ , shown on Fig. 1(b).

As a starting step of our analysis, we consider only the “extreme” intensity fluctuations by selecting an adequate

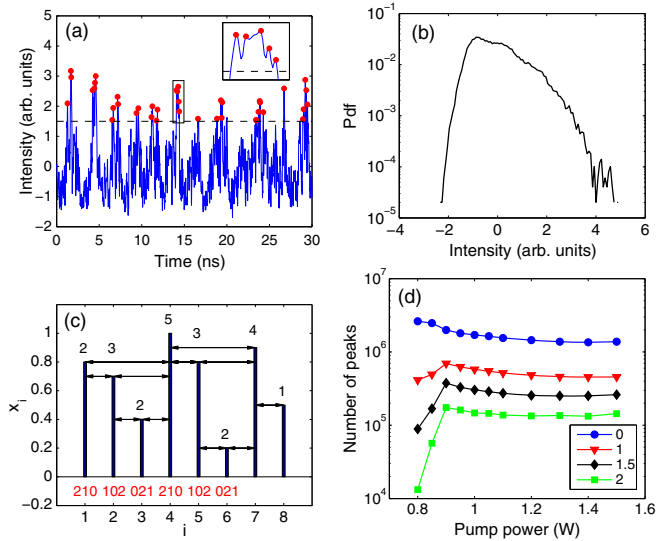


FIG. 1. (a) Stochastic dynamics of a quasi-cw Raman fiber laser: intensity time series measured at pump power 0.9 W (the dots indicate the peak values above a threshold, indicated with a dashed line, and the inset displays a detail). (b) PDF of the intensity values. (c) Schematic representation of the two analysis methods: the values  $\{x_i\}$  in a time series are represented with vertical bars, the ordinal patterns formed by  $(x_i, x_{i+1}, x_{i+2})$  are indicated in red, the links in horizontal visibility graph are indicated with arrows, and the numbers indicate the degree (the number of links) of each data point (graph node). (d) Number of intensity peaks vs the pump power for various thresholds (threshold values are shown by different colors).

threshold, and filter out the intensity peaks whose height is below the threshold, as shown in Fig. 1(a). Thus, we keep a sequence of intensity peaks heights,  $\{I_{\max,i}\}$ , which are above the threshold, and also consider the sequence of time intervals between these peaks. In this way, we generate two new data sets from the experimentally measured intensity dynamics. Naturally, the precise definition of “extreme” fluctuations depends on the system under investigation. In hydrodynamics, when the height of a wave is larger by a factor of 3 than average, this wave is considered extreme, but in optics, fluctuations of much higher amplitudes compared to the average can often be observed. Here, because each time series is normalized to zero mean and unit variance, the thresholds used are in units of the standard deviation  $\sigma$ .

The number of peaks found in intensity dynamics measured at different pump power level is shown on Fig. 1(d) depending on the threshold value. The transition between the laminar and turbulent regimes is clearly detected at 0.9 W. In the following we analyze only the intensity peaks that are above  $2\sigma$ . As shown in the Supplemental Material [20], our results are robust for other threshold choices. As each local intensity peak has also a time instant  $T_i$  at which it occurs, we generate another data

set: a sequence of time intervals between local intensity peaks  $\{\Delta T_i\}$ .

The methods used to analyze the data are represented schematically in Fig. 1(c). Ordinal analysis [9] transforms a time series  $\{x_i\}$  (where  $\{x_i\}$  is either the sequence of peak heights  $\{I_{\max,i}\}$  or the sequence of time intervals between peaks  $\{\Delta T_i\}$ ) into a sequence of symbols (referred to as ordinal patterns, OPs), by considering the order relation among  $D$  values of the time series. For example, there are 2 different ordinary patterns of length 2: pattern “01” if  $x_i < x_{i+1}$  and pattern “10” if  $x_i > x_{i+1}$ . If  $D = 3$ , there are 6 possible patterns:  $x_i < x_{i+1} < x_{i+2}$  gives “012,”  $x_{i+2} < x_{i+1} < x_i$  gives “210,” etc. The number of possible patterns of the given length  $D$  is  $D!$ . In this way, a sequence of patterns could be generated from the sequence of the peak heights or from the sequence of time intervals between the peaks.

After defining the sequence of patterns, one can calculate the probability to find the given pattern in the data set,  $p_i$ . The entropy computed from their probabilities  $p_i$  of occurrence in the time series,  $S_{\text{PE}} = -\sum p_i \log p_i$ , known as permutation entropy, has been shown to be an appropriated measure of the complexity of a time series [9,12,13]. When there are no serial correlations in the time series  $\{x_i\}$ , then all the patterns are equally probable and  $S_{\text{PE}} \sim \log D!$ . On the contrary, when there are serial correlations, then the OPs are not all equally probable, and the permutation entropy will be  $S_{\text{PE}} < \log D!$ . In the following we refer to the normalized entropy  $S_{\text{PE}}/\log D!$  as PE entropy. Thus, with an appropriate choice of pattern length  $D$ , the OP probabilities, and the PE entropy will capture the existence of underlying correlations in the time series.

To verify independently the presence of correlations, we also apply the HVG method [10] that converts a time series  $\{x_i\}$  into a graph by considering each data point  $x_i$  as a node. Any two nodes are connected if it is possible to trace a horizontal line linking  $x_i$  and  $x_j$  not intersecting intermediate data [see Fig. 1(c)]; mathematically, this means that  $x_i$  and  $x_j$  are connected if  $x_i, x_j > x_n$  for all  $i < n < j$ . Note that this graph representation of the time series  $\{x_i\}$  takes into account both the order and the values of the data points. Time series with different dynamics are mapped into graphs that exhibit distinct topological structures [14]. The topology of a graph is characterized by the degree distribution  $p(k)$  that is the probability that a node has  $k$  links. Thus, the entropy of the degree distribution,  $S_{\text{HVG}} = -\sum p_k \log p_k$  (in the following, referred to as HVG entropy), is another complexity measure normalized here to the entropy of Gaussian white noise [18] (see Supplemental Material [20]).

The HVG method also allows us to analyze different time scales by constructing the graph not from all the “raw” data points, but from lagged data  $\{x_i, x_{i+\tau}, x_{i+2\tau}, \dots\}$ .

Both analysis methods share the common feature of transforming the time series  $\{x_i\}$  into a sequence of integer

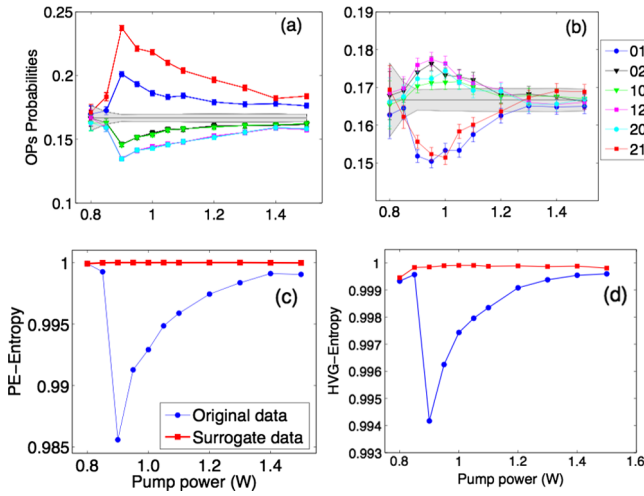


FIG. 2. Probabilities of ordinal patterns of length  $D = 3$  vs the pump power calculated from the sequence of (a) intensity peaks and (b) time intervals between consecutive peaks. The error bars are computed with a binomial test and the gray region indicates probability values consistent with the uniform distribution (see Supplemental Material [20] for details). PE entropy (c) and HVG entropy (d) calculated from the sequence of intensity peaks, original and shuffle data.

numbers,  $\{k_i\}$  (in the OP case,  $k_i \in [1, D!]$  is the pattern label: if 01,  $k_i = 1$ ; if 10,  $k_i = 2$ , etc.; in the HVG case,  $k_i \in [1, N - 1]$  is the degree of  $x_i$ , with  $N$  being the number of data points in the time series). But, while the OP method requires the predefinition of the length of the pattern  $D$ , and does not take into account the values of the data points, the HVG method does not require to predefine an analysis length, and considers both, the order relation and the actual values of the data points.

Figures 2(a) and 2(b) display the probabilities of the six patterns of length 3 calculated from the sequence of intensity peaks and from the sequence of the time intervals, respectively.

We observe that the variation of the probabilities with the pump power captures the transition between two dynamical regimes: below the transition the OPs are equally probable, while during the transition from laminar to turbulent regime their probabilities are different from equiprobability. We also note that the patterns calculated from the intensity peaks capture more determinism than those computed from the time intervals [notice the difference in the vertical scales of Figs. 2(a) and 2(b)]. This indicates that the timing of the high intensity peaks is more random than their peak values.

The PE entropy Fig. 2(c) quantifies this effect by decreasing sharply at the transition power. A similar behavior is observed when computing the HVG entropy, Fig. 2(d). In both cases, the entropy values computed from surrogate data obtained by shuffling the values of the data points in the original time series, are also indicated. One can observe that, as expected, the transition is not detected in the shuffle data. In Fig. 2(c) the PE entropy was

computed from  $D = 3$  OPs; similar plots were obtained with  $D \in [2-6]$  (see Supplemental Material [20]).

To investigate the presence of specific time-scales in the dynamics, we analyze the lagged time series, i.e., the sequence of  $\{I_i, I_{i+\tau}, I_{i+2\tau}, \dots\}$ , where  $\tau$  is the lag time. We begin by considering the case  $\tau = 1$  (i.e., we analyze all data points). Figure 3(a) displays the PE entropy and the HVG entropy vs the pump power, and same behavior is seen in both entropies: there is a clear transition at pump power 0.9 W, where both entropies smoothly decrease. It is also observed that for the highest pump power, both entropies increase again. This reveals that during the transition there is an increase in the “ordering” of consecutive intensity values (that is captured by both entropies, which decrease), but for the highest pump power the trend reverses and the disorder increases. In contrast, the entropy computed in the conventional way and referred as PDF entropy [i.e., the entropy calculated from the intensity PDFs of the initial intensity dynamics,  $I(t)$ ] does not capture this behavior: as it can be seen in Fig. 3(b), after the transition the PDF entropy monotonically decreases with the pump power. Thus, the PE and HVG entropies provide consistent information, which complements that gained from the standard PDF entropy. The good agreement between the two entropies, also seen in Figs. 2(c) and 2(d), is remarkable because the two methods transform a time series into a sequence of integer numbers by using very different encoding rules.

By varying the value of the lag time  $\tau$ , i.e., by taking into account not all points in data sets, but every second ( $\tau = 2$ ) point, every third ( $\tau = 3$ ) point, etc., we are able to identify a specific oscillation time scale in the intensity time-series during the transition. The PE entropy vs  $\tau$  for pump powers below (0.85 W), at (0.90 W), and above (0.95 W) the transition is displayed in Fig. 4(a). Here we can notice that, at the transition, there are specific lags for which the PE entropy decreases sharply. Similar results were obtained with the HVG entropy.

The sharp minima indicates that, for pump power 0.90 W and for specific lags, 6 different patterns of length  $D = 3$

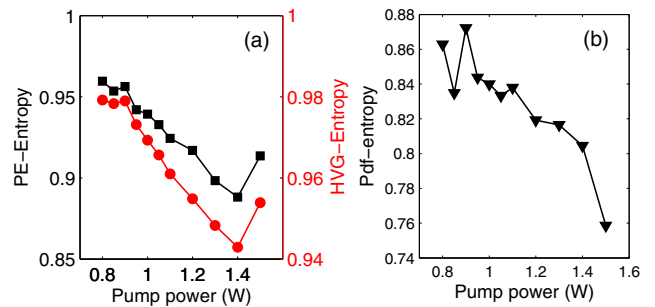


FIG. 3. (a) Permutation entropy (black) and HVG entropy (red) vs the pump power. Calculations are performed with  $D = 3$  OPs. (b) PDF entropy calculated from the distribution of intensity values.

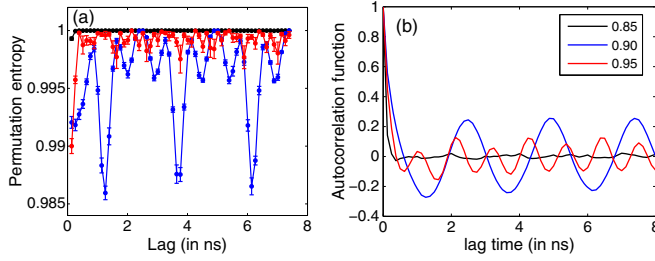


FIG. 4. (a) Permutation entropy vs the lag time before (0.85), at (0.9), and after (0.95 W) the transition to optical turbulence. Error bars were computed by dividing the data in 10 windows and computing the PE entropy in each window. (b) Autocorrelation function vs lag, for the same pump powers as panel (a).

are not all equally probable, and thus, there are serial correlations in the sequence of lagged intensity values. To explore the length of such correlations, we computed the PE entropy using longer ordinary patterns ( $D = 4$  and  $D = 6$ ) and found that the minima were more pronounced, revealing the existence of long serial correlations. These correlations are not captured by the classical autocorrelation function shown in Fig. 4(b) for comparison purposes, which displays only a smooth variation with  $\tau$ .

To investigate the nature of these correlations we plot in Fig. 5(a) how the probabilities of 6 different ordinary patterns of length  $D = 3$  depend on the lag time. We note a periodic alternation in which 012 and 210 became the more probable or the less probable patterns. The probabilities of the other four patterns are similar (no clear clusters are

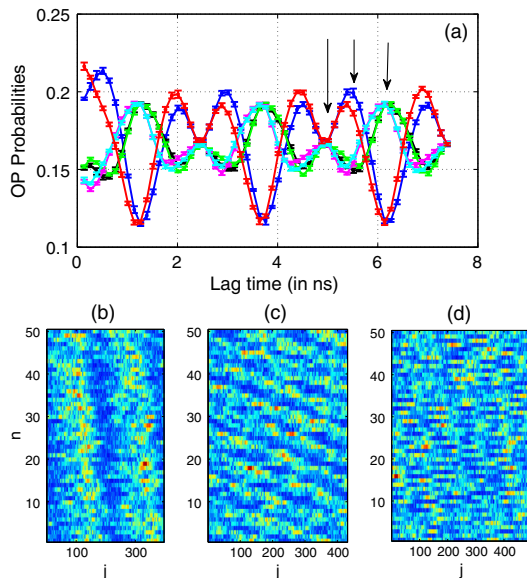


FIG. 5. (a) Probabilities of the ordinary patterns of length  $D = 3$  vs lag time  $\tau$ . (b)–(d) Spatiotemporal structures identified with the specific lags indicated with arrows in panel (a). The color scale indicates the value of  $I_i$  with  $i = n\tau + j$  and  $\tau = 396, 431$ , and  $496$  in units of the sampling time. The pump power is  $0.9$  W.

seen). The lag values for which 012 and 210 are less probable correspond, as expected, to the lag values where the autocorrelation function is minimum (and negative). However, unexpectedly, the lag values for which 012 and 210 are more probable, do not correspond to the maxima of the autocorrelation, and moreover, for the lag values where the autocorrelation is maxima, all six ordinary patterns have similar probabilities. These observations suggest that ordinal analysis identifies subtle correlations in the *ordering* of data points, which are not seen by the standard autocorrelation function, that measures correlations in the *values* of the data points.

These “order correlations” result in different types of spatiotemporal patterns. Let us recall that the intensity time series can be represented as a spatiotemporal plot, by choosing an appropriate characteristic time scale [21–23]. Here we apply this concept and choose specific lag times defined from Fig. 5(a) (shown by arrows) to be used as characteristic time scales. Figures 5(b)–5(d) display examples with lags such that patterns 012 and 210 are as probable [Fig. 5(b)], more probable [Fig. 5(c)], and less probable [Fig. 5(d)] than the other four patterns. We can see that these spatiotemporal dynamics of patterns display clear and different coherent structures. These observations can be useful for confronting the predictions of state-of-the-art laser models with empirical data, and the theoretical studies could provide insight into the physical mechanisms underlying these correlations.

To summarize, by applying two independent tools of nonlinear time-series analysis we have uncovered long-range temporal correlations in the intensity output of a fiber laser during the transition to a wave turbulence regime. Output of laser radiation is easily measurable, making these easily implementable methods useful and valuable techniques for investigating coherent structures in complex laser radiation. Both approaches can be applied to any high-dimensional complex systems that undergo similar transitions accompanied by the generation of extreme fluctuations.

This work has been supported by the ERC project ULTRALASER, the Ministry of Education and Science of the Russian Federation (Agreement No. 14.B25.31.0003), the Spanish MINECO (FIS2012-37655-C02-01), European Office of Aerospace Research and Development (EOARD) (Grant No. FA9550-14-1-0359), CNPq Brazil, Russian Foundation for Basic Research (Grant No. 15-02-07925), Presidential Grant for Young researchers (Grant No. 14.120.14.228-MK). N. T. is supported by the Russian Science Foundation (Grant No. 14-21-00110).

- [1] C. J. S. de Matos, L. de S. Menezes, A. M. Brito-Silva, M. A. Martínez Gámez, A. S. L. Gomes, and C. B. de Araújo, *Phys. Rev. Lett.* **99**, 153903 (2007).

- [2] S. K. Turitsyn, J. D. Ania-Castanon, S. A. Babin, V. Karalekas, P. Harper, D. Churkin, S. I. Kablukov, A. E. El-Taher, E. V. Podivilov, and V. K. Mezentsev, *Phys. Rev. Lett.* **103**, 133901 (2009).
- [3] S. K. Turitsyn, S. A. Babin, D. V. Churkin, I. D. Vatik, M. Nikulin, and E. V. Podivilov, *Phys. Rep.* **542**, 133 (2014).
- [4] A. El-Taher, O. Kotlicki, P. Harper, S. Turitsyn, and J. Scheuer, *Laser Photonics Rev.* **8**, 436 (2014).
- [5] D. V. Churkin, A. E. El-Taher, I. D. Vatik, J. D. Ania-Castañón, P. Harper, E. V. Podivilov, S. A. Babin, and S. K. Turitsyn, *Opt. Express* **20**, 11178 (2012).
- [6] A. Picozzi, J. Garnier, T. Hansson, P. Suret, S. Randoux, G. Millot, and D. N. Christodoulides, *Phys. Rep.* **542**, 1 (2014).
- [7] *Advances In Wave Turbulence*, World Scientific Series on Nonlinear Science: Series A, edited by V. Shrira and S. Nazarenko (World Scientific, Singapore, 2013).
- [8] E. G. Turitsyna, S. V. Smirnov, S. Sugavanam, N. Tarasov, X. Shu, S. A. Babin, E. V. Podivilov, D. V. Churkin, G. E. Falkovich, and S. K. Turitsyn, *Nat. Photonics* **7**, 783 (2013).
- [9] C. Bandt and B. Pompe, *Phys. Rev. Lett.* **88**, 174102 (2002).
- [10] B. Luque, L. Lacasa, F. Ballesteros, and J. Luque, *Phys. Rev. E* **80**, 046103 (2009).
- [11] C. Bandt and F. Shiha, *J. Time Ser. Anal.* **28**, 646 (2007).
- [12] M. Zanin, L. Zunino, O. A. Rosso, and D. Papo, *Entropy* **14**, 1553 (2012).
- [13] J. M. Amigo *et al.*, *Eur. Phys. J. Spec. Top.* **222**, 241 (2013).
- [14] L. Lacasa and R. Toral, *Phys. Rev. E* **82**, 036120 (2010).
- [15] J. B. Elsner, T. H. Jagger, and E. A. Fogarty, *Geophys. Res. Lett.* **36**, L16702 (2009).
- [16] M. Ahmadlou, H. Adeli, and A. Adeli, *Journal of neural transmission* **117**, 1099 (2010).
- [17] U. Parlitz, S. Berg, S. Luther, A. Schirdewan, J. Kurths, and N. Wessel, *Computers in Biology and Medicine* **42**, 319 (2012).
- [18] M. Gomez Ravetti, L. C. Carpi, B. Goncalves, A. C. Frery, and O. A. Rosso, *PLoS One* **9**, e108004 (2014).
- [19] A. Aragonese, S. Perrone, T. Sorrentino, M. C. Torrent, and C. Masoller, *Sci. Rep.* **4**, 4696 (2014).
- [20] See Supplemental Material at <http://link.aps.org/supplemental/10.1103/PhysRevLett.116.033902> for details regarding the robustness of the results with respect to the choice of thresholds and pattern lengths. The Supplemental Material also includes information about the computation of error bars in ordinal patterns probabilities plots.
- [21] D. V. Churkin, S. Sugavanam, N. Tarasov, S. Khorev, S. V. Smirnov, S. M. Kobtsev, and S. K. Turitsyn, *Nat. Commun.* **6**, 7004 (2015).
- [22] J. K. Jang, M. Erkintalo, S. Murdoch, and S. Coen, *Nat. Photonics* **7**, 657 (2013).
- [23] B. Garbin, J. Javaloyes, G. Tissoni, and S. Barland, *Nat. Commun.* **6**, 5915 (2015).